SCIENTIFIC REPORTS

OPEN

Strain glass state as the boundary of two phase transitions

Zhijian Zhou[1], Jian Cui[1] & Xiaobing Ren[1,2]

A strain glass state was found to be located between B2-B19' (cubic to monoclinic) phase transition and B2-R (cubic to rhombohedral) phase transition in $Ti_{49}Ni_{51}$ alloys after aging process. After a short time aging, strong strain glass transition was observed, because the size of the precipitates is small, which means the strain field induced by the precipitates is isotropic and point-defect-like, and the distribution of the precipitates is random. After a long time aging, the average size of the precipitates increases. The strong strain field induced by the precipitates around them forces the symmetry of the matrix materials to conform to the symmetry of the crystalline structure of the precipitates, which results in the new phase transition. The experiment shows that there exists no well-defined boundary in the evolution from the strain glass transition to the new phase transition. Due to its generality, this glass mediated phase transition divergence scheme can be applied to other proper material systems to induce a more important new phase transition path, which can be useful in the field of phase transition engineering.

Ti-Ni shape memory alloys have attracted much interest in the past decades due to their excellent functional properties such as shape memory effect and superelasticity[1]. Stoichiometric $Ti_{50}Ni_{50}$ alloy undergoes a phase transition from B2 (cubic) structure to B19' (monoclinic) structure at 50 °C. However, many factors can alter the phase transition path. Some other structures may be involved, such as rhombohedral (R) phase, B19 (orthorhombic) phase. When Ni is replaced by Cu, B2-B19' phase transition changes to B2-B19 phase transition when Cu concentration exceeds 15%[2]. When Ni is replaced by Cr, Mn, Fe or Co above certain concentrations, B2-B19' phase transition changes to B2-R-B19' or B2-R phase transition[3–6]. Also, aging process can change the phase transition from B2-B19' to B2-R-B19' or B2-R for TiNi alloys with excessive Ni atoms[7,8]. It is thought that the transition from one phase transition path to another one is not a abrupt process, so it is expected that there might exist a transitional region in between the change of phase transition paths to be discovered.

In TiNi system, it is very hard to see the details of the change from on phase transition to another one, because the composition range to induce the change of phase transition path is very small (<1%)[4–6,9]. Alternatively, aging process can effectively prolong the procedure by selecting proper aging temperature and aging time, so that it is possible to observe very fine details during the change of phase transition paths. In TiNi system, the aging process has been studied at various temperatures[7,8,10–12]. Fan et al.[7], Zhou et al.[8], and Zheng et al.[10] used relatively long aging time (>1 hour), so that B2-R phase transition appears abruptly. Wagner et al.[11] used thermal cycling technique to study the effect of precipitates induced by low temperature aging on the phase transition. However they did not focus on the phenomena with short time thermal treatment. Kim et al.[12] mainly studied the microstructure of precipitates by low and high temperature aging. In this study, we adopted a low aging temperature (280 °C) and monitored the aging time dependence of phase transition process, so that we can capture the snapshots of the material during the evolution from B2-B19' to B2-R-B19' at very early stage.

The result shows that at the initial aging stage, strong strain glass transition can be observed. With the increase of aging time, B2-R phase transition gradually forms. After a short time aging, the average size

[1]Multi-Disciplinary Materials Research Center, Frontier Institute of Science and Technology, Xi'an Jiaotong University, 710054 Xi'an, China. [2]Ferroic Physics Group, National Institute for Materials Science, 1-2-1 Sengen, Tsukuba, Ibaraki 305-0047, Japan. Correspondence and requests for materials should be addressed to J.C. (email: tsuijian@gmail.com)
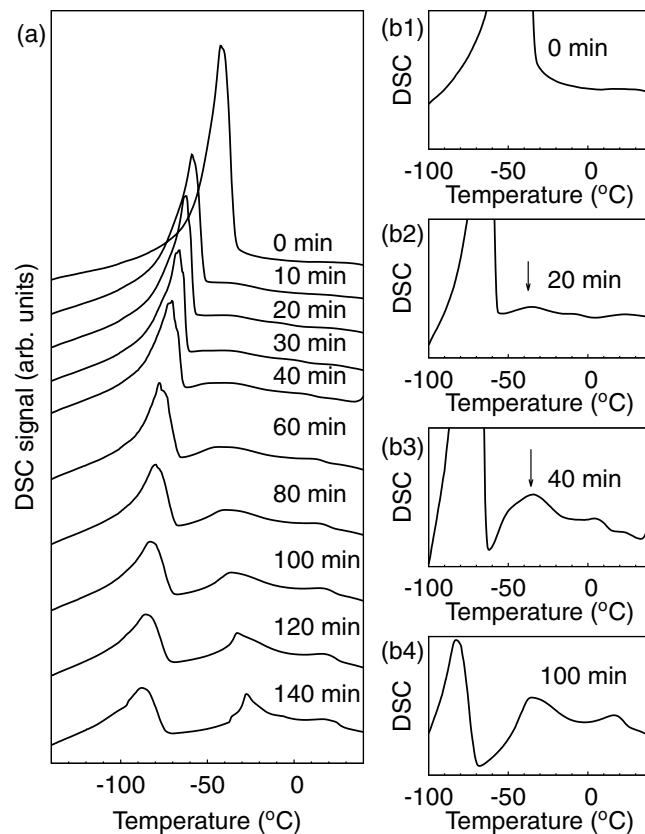
Figure 1. DSC curves of Ti$_{49}$Ni$_{51}$ alloys aged for various times. (a) Aging-time dependence of cooling DSC curves of aged Ti$_{49}$Ni$_{51}$ alloys for different times. **(b1)–(b4)** The magnified DSC curves in **(a)** for 4 typical aging times. The arrows indicate the weak broad humps, which correspond to the strain glass transitions in aging process.

of the precipitates is small (point-defect-like) and distribution is random, which results in the formation of strain glass transition. After a long time aging, the average size of the precipitates becomes large. The strong strain field induced by the precipitates around them forces the symmetry of the matrix materials to conform to the symmetry of the crystalline structure of the precipitates at low temperatures, which results in the new phase transition. No well-defined boundary exists in the evolution from the strain glass transition to the new phase transition. The divergence of a phase transition to another phase transition by point defect doping is widely observed and martensite to strain glass transition is also widely found. Our finding about the glass mediated phase transition divergence may provide new clues to study the boundary between two transitions while doping or aging.

Results

Figure 1 displays the differential scanning calorimetry (DSC) curves of Ti$_{49}$Ni$_{51}$ alloys aged at 280 °C for different times. The average grain size of the samples was about 50 μm from optical microscopy, so that there is no size effect on the measured properties. For the as-quenched sample, only one sharp DSC peak was observed, which corresponds to the phase transition from B2 to B19' structure. With aging time increasing further, the sharp DSC peak continuously shifted towards low temperature and became broad and weak. It is interesting to notice that after aging for a short time, one broad weak hump appeared at the temperature which is a little higher than the transition temperature of B2-B19'. A typical case is shown in Fig. 1(b2). With aging time increasing further, a new broad hump appeared, as shown in Fig. 1(b3). By aging for a longer time, the broad hump gradually became sharp. Finally, an apparent two-stage phase transition was formed. Because the aging time is a continuous parameter, the appearance of the new phase transition is not a abrupt change but a gradually evolving process.

The new phase transition is considered to be the phase transition from B2 to R phase, since in previous studies[7,8], after long time aging (aging for over 60 min) B2-R phase transition was observed at higher temperatures. As we know, accompanying a first-order phase transition latent heat is released when cooling and absorbed when heating, in which a strong peak features in DSC curves. It is hard to say the broad humps observed in short time aging corresponds to a first-order phase transition. Then it is very interesting to ask what corresponds to these broad humps.
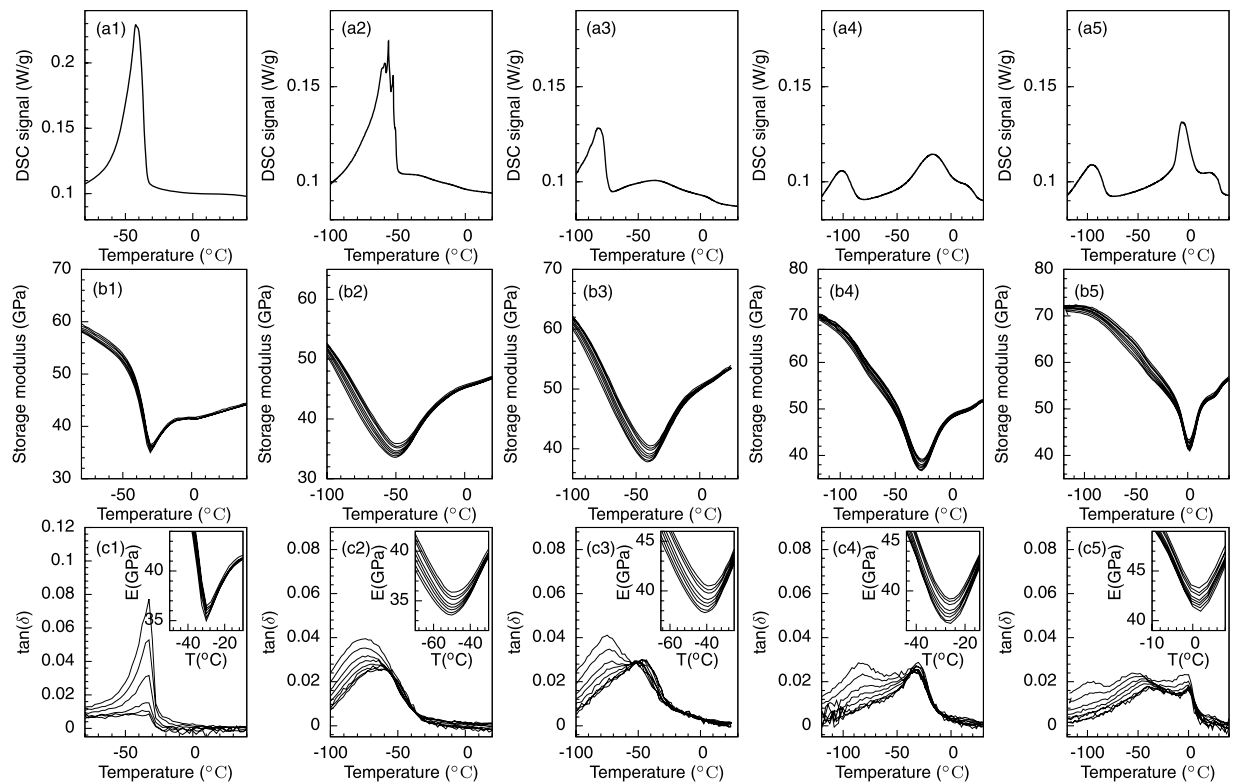
Figure 2. Summary of the thermal and mechanical characterizations. DSC curves ((a1)–(a5)), Storage modulus ((b1)–(b5)) and tan(δ) ((c1)–(c5)) of $Ti_{49}Ni_{51}$ alloys aged for 0 min ((a1)–(c1)), 10 min ((a2)–(c2)), 30 min ((a3)–(c3)), 60 min ((a4)–(c4)) and 180 min ((a5)–(c5)), respectively. The insets in (c1)–(c5) are the magnifications of (b1)–(b5) in the corresponding temperature region, which manifest the frequency dependence of the modulus dip.

In order to elucidate the physical nature of these broad humps, dynamic mechanical analysis (DMA) experiments were performed. The results are summarized in Fig. 2. For the sample without aging, strong DSC peak, strong storage modulus softening and strong internal friction are observed at the same temperature of −30 °C (shown in Fig. 2(a1,b1,c1)). Figure 2(a2) shows the DSC curve of the sample aged for 10 min, in which a small hump appears at the temperature a little above the main phase transition temperature. Correspondingly, the storage modulus behavior is modified. Frequency dispersion of storage modulus is clearly observed, as shown in the inset of Fig. 2(c2). The internal friction (tan(δ)) also shows two close peaks (Fig. 2(c2)), which correspond to the hump and the peak in the DSC curve. After aging for 30 min, the temperature gap between the hump and the main phase transition is enlarged, as shown in Fig. 2(a3). The hump becomes apparent. The storage modulus dip excellently corresponds to the hump by comparing Fig. 2(a3,b3). The internal friction shows two corresponding separate peaks (Fig. 2(c3)). Frequency dispersion of storage modulus is also observed in the inset of Fig. 2(c3). After aging for 60 min, the hump develops into a broad peak, as shown in Fig. 2(a4). The storage modulus dip corresponds to the developed peak. The correspondence between DSC hump/peak and internal friction persists, while the frequency dispersion of storage modulus is reduced compared with the samples aged for short times. After aging for 180 min, the previous hump develops into a sharp peak and the frequency dispersion of storage modulus nearly does not observed, as shown in Fig. 2(a5) and inset in Fig. 2(c5). It is noted that the internal friction peak at around −50 °C in Fig. 2(c5) may originate from the hydrogen relaxation induced by long time aging.

Frequency dispersion of storage modulus and internal friction is a main feature of strain glass[4,5,9,13]. Similar phenomena can also be observed in other ferroic glass transition, e.g. spin glass and relaxor ferroelectrics. The observed frequency dispersion of storage modulus and internal friction in $Ti_{49}Ni_{51}$ alloys aged for a short time strongly suggest the appearance of strain glass transition therein, which was confirmed by temperature dependence of x-ray diffraction (XRD) spectra. For the virgin $Ti_{49}Ni_{51}$ sample, B2-B19' transition is clearly shown in Fig. 3(a). Typical B19' XRD peaks can be observed at low temperatures. From Fig. 3(b), by aging for 10 min for the $Ti_{49}Ni_{51}$ sample, it is interesting to notice that when the temperature decreases to −40 °C, some weak peaks can be observed. These peaks are very close to the B19' XRD peaks while they are different, by comparing with Fig. 3(a). At the same time, the (110)B2 peak becomes a little broader. When the temperature decreases further, these peaks develop continuously
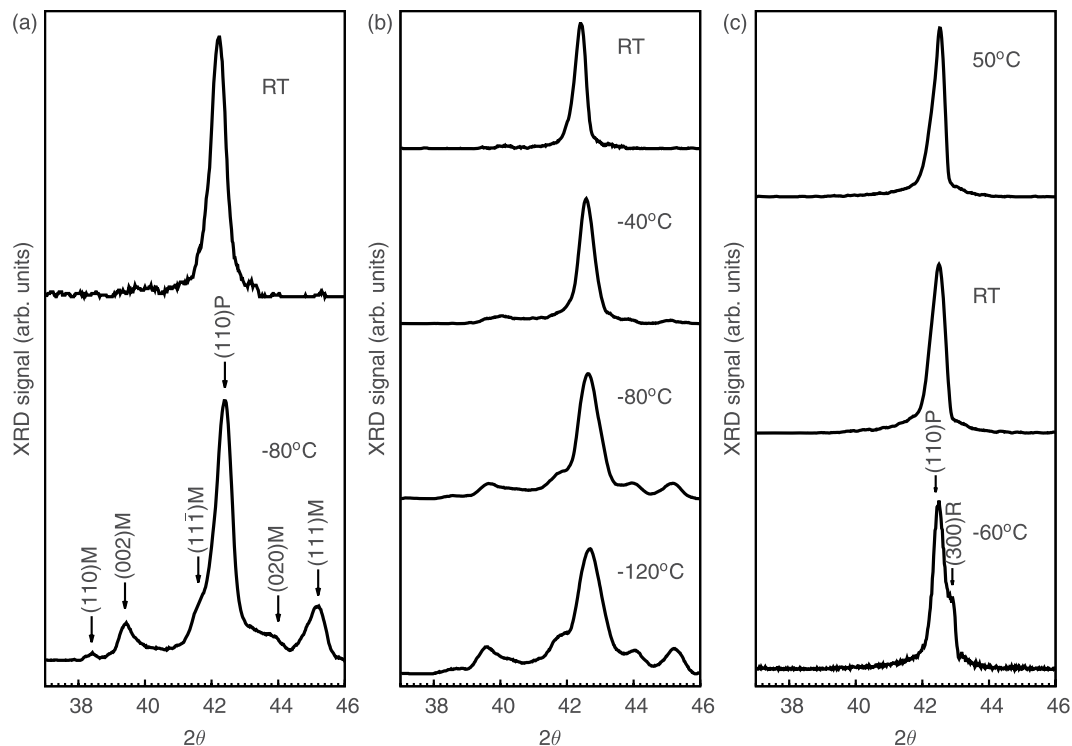
Figure 3. Temperature dependence of XRD spectra. (**a**) XRD spectra for $Ti_{49}Ni_{51}$ alloys without aging process. (**b**–**c**) XRD spectra for $Ti_{49}Ni_{51}$ alloys aged for (**b**) 10 min and (**c**) 180 min.

into the peaks corresponding to B19' structure and the (110)B2 peak becomes broader. After aging for 180 min for the $Ti_{49}Ni_{51}$ sample, B2-R structural transition can be identified, as shown in Fig. 3(c), which is very similar to case of Fe doped TiNi alloys[5,14].

For the $Ti_{49}Ni_{51}$ sample aged for 10 min, at $-40\,°C$ the material is in a strain glass state but still before the phase transition as shown in Fig. 2(a2–c2). The observed weak B19'-like peaks and the broaden (110) B2 peak as shown in Fig. 3(b) are all the features of a glass state because though the overall structure does not change, which indicates that the XRD peaks of parent phase dominate during cooling down to low temperature[4,5,9,13], the crystal lattices are distorted locally, which indicates that the XRD peaks of parent phase may be broadened or martensite-like XRD peaks arise[5,14].

The frequency dispersion of storage modulus induced by strain glass transition can be modeled by Vogel-Fulcher formula due to its glass nature[15,16], as follows:

$$\omega = \omega_0 \times e^{-\frac{E_a}{k_B(T_g - T_0)}} \tag{1}$$

where ω is the frequency used in measurement, ω_0 a constant, E_a the activation energy, k_B the Boltzmann constant, T_g the freezing temperature with frequency ω which is taken as the temperature at the dip of the storage modulus, T_0 the glass transition temperature. The frequency dependence of the $Ti_{49}Ni_{51}$ alloys aged for various times is presented in Fig. 4(a). It can be found that the experimental results can be fitted by Eq. (1) very well. From Eq. (1), it can be seen that the activation energy E_a characterizes the extent of frequency dispersion for a glass transition. The larger E_a is, the more apparent the glass transition is. For the four samples, E_a vs. aging time is presented in Fig. 4(b). It can be seen that by aging for a very short time, apparent glass transition appears. With the aging time increasing further, E_a experiences a peak and then gradually decreases to nearly zero.

According to the experimental results and analysis, the phase diagram of $Ti_{49}Ni_{51}$ upon aging time can be drawn, which is shown in Fig. 5. Upon cooling, a strain glass region in transitional region with short aging time can be identified. The strain glass transition temperature (blue line in Fig. 5), are taken as the boundary between B2 and strain glass state. By aging for above 120 min, we can say that clear B2-R phase transition appears, where the starting temperature for B2-R transition (Rs) is well defined. The observable weak peak near room temperature in Fig. 5 corresponds to the B2-R phase transition induced by the precipitates around crystal boundaries[7,8].

It is known that the main physical process in aging for $Ti_{49}Ni_{51}$ alloys is the formation of precipitates[7,8], which are Ti_3Ni_4. The atomic structure of Ti_3Ni_4 precipitates was firstly identified to be the rhombohedral structure with $a = 0.670$ nm, $\alpha = 113.9°$[17], or in the hexagonal description with $a = b = 1.124$ nm,
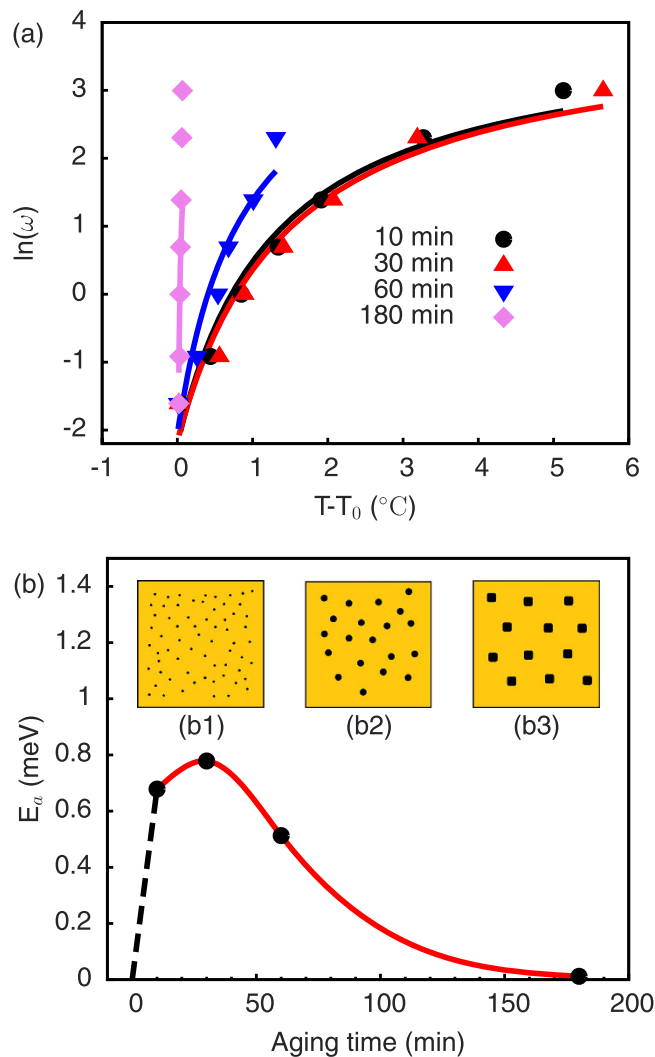
Figure 4. Frequency dependence of freezing temperature and the derived activation energy vs. aging time. (**a**) Frequency dependence of the freezing temperature (symbols) and Vogel-Fulcher fitting results (lines) for the samples aged from 10 to 180 min. The experimental data are extracted from Fig. 2. (**b**) The relation between aging time and the activation energy obtained from Vogel-Fulcher fitting results in (**a**). For unaged sample, because only pure phase transition is presented, E_a is considered to be zero. The line is a guide for the eye. (b1)–(b3) schematically show the evolution of the microscopic structures in aging process. (b1) For short time aging, small precipitates randomly distribute in the matrix of the alloy. (b2) With aging time increasing, the size of precipitates increases and the density decreases. (b3) With long enough aging time, the size of the precipitates and the density tend towards saturation.

$c = 0.5077\,\text{nm}$[18]. The atomic structure was also refined by electron diffraction[19] and neutron diffraction[20] and the rhombohedral structure was confirmed. It is shown that the structure of Ti_3Ni_4 is a slight modification of the B2 structure of matrix[17], so the strain field induced by the precipitates is relatively small. Thus the precipitates locate in the matrix coherently[21]. The size of the precipitates in the whole aging times is below 10 nm[12,22], and distribution of the precipitates is homogeneous[8].

The strain glass formation is considered to be caused by the point defects doped in ferroelastic materials, which disturb the long range ordering of the matrix materials[23]. For aged $Ti_{49}Ni_{51}$ alloys, the same theory can be applied. The size and distribution of the precipitates during aging process evolve with aging time, and consequently influence the mechanical properties. The precipitate development procedure can be divided into 3 stages, as shown in Fig. 4(b1–b3). At the initial stage, large amount of small precipitates randomly distributed are created. At the next stage, the small precipitates coalesce together and larger precipitates are formed. At the final stage, the size of the large precipitates tends to a saturated value. This scheme is a typical nucleation and self-assembly growth process and has been confirmed by transmission electron microscopy[12].

The functions of the precipitates at different stages determine the formation of strain glass transition and B2-R phase transition. At the first stage, due to the small size of the precipitates, the strain field
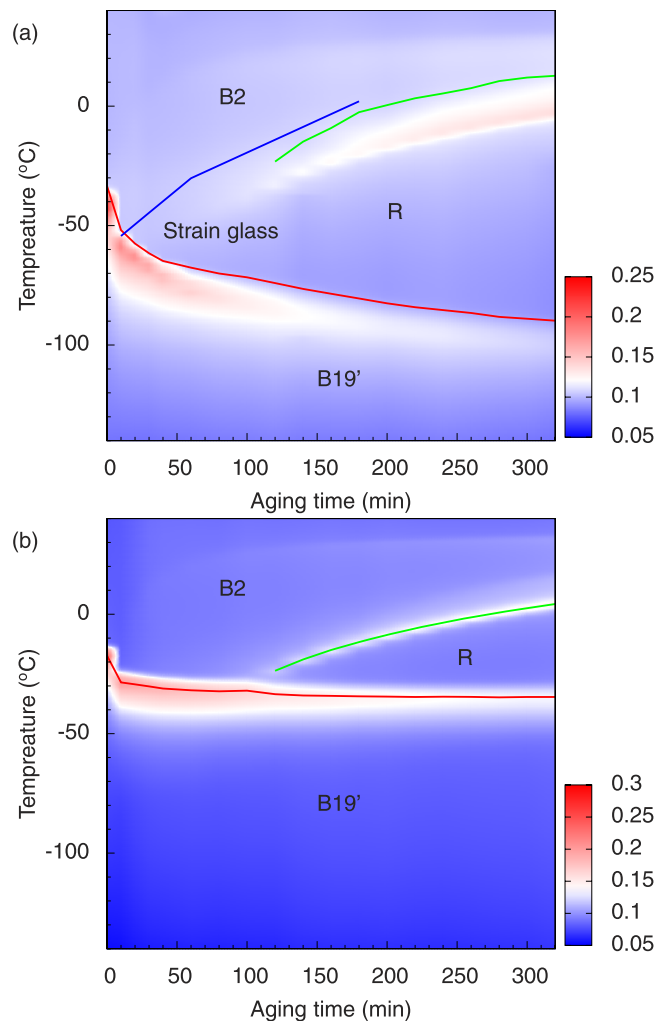
Figure 5. Temperature-aging time phase diagram of Ti$_{49}$Ni$_{51}$ alloys. The phase diagrams are obtained in cooling (**a**) and heating processes (**b**), respectively. In (**a**), the red line indicates Ms for B2/R-B19', the green line indicates the Rs for B2-R and the blue line indicates the strain glass transition temperature obtained by fitting with Eq. (1). In (**b**), the lines are the connecting lines of the DSC peaks for B19'-B2/R (red line) and R-B2 (green line), respectively. The color bar indicates the absolute value of the measured heat flow intensity in the unit of W/g.

induced by the precipitates is nearly isotropic and thus the function of the precipitates is very similar to the point defects as in doped TiNi alloys[23]. So we observed strong strain glass transition at this stage with the help of the random distribution of the precipitates. With the increase of the size of the precipitates after long time aging, the strain field induced by the precipitates gradually increases, which forces the crystalline symmetry of the B2 matrix to conform to the symmetry of the precipitates. The free energy balance between B2 parent phase and R product phase induced by Ti$_3$Ni$_4$ precipitates determines the phase transition temperature. As the size of the precipitates saturates, the B2-R phase transition temperature tends to saturate too, which is consistent with our result as shown in Fig. 5. Under this condition, nearly all the matrix will transform into R phase due to strong strain field induced by large precipitates, thus we observed clear B2-R phase transition.

It is interesting to note that our result reveals the fine details of the phase transition evolution from one-step phase transition to two-step phase transition, as shown in Fig. 5. The result not only fills the blank area in the previous study[7,8], but also presents a general way to diverge a phase transition path, which may be applied to other materials by introducing precipitates with different symmetry to the matrix materials. By using various precipitates with desired crystalline symmetry, the phase transition path can be manipulated, which provides the freedom in phase transition engineering. Our result points out a general way to design new desired phase transition path in a matrix material, e.g. in Fe-based alloys. It is considered that the same mechanism can be applied for FeNiCoAlTa ferrous shape memory alloys[24]. The details will be reported elsewhere.

In conclusion, we have investigated the phase transition divergence of $Ti_{49}Ni_{51}$ alloy by aging process. The new B2-R phase transition gradually emerges after aging. A strain glass region was observed in the phase diagram located between B2-B19' phase transition and B2-R phase transition. The corresponding microscopic mechanism is attributed to the different functions of the precipitates for various aging times. After a short time aging, the size of precipitates is small, the population is large and the distribution is random. Under this condition, a strain glass transition forms for the precipitates act like isotropic point defects. After a long time aging, the strong strain field induced by large precipitates around them forces the symmetry of the matrix material to conform to the symmetry of the precipitates. Under this condition, a new phase transition forms. But there is no clear boundary in the evolution from the strain glass transition to the new phase transition. Our result clarifies the physical origin of the formation of B2-R phase transition, which is omitted in previous works. Our study shows that a new phase transition can be induced by introducing proper precipitates. The phase diagram we presented is rather general and might exist widely in other ferroelastic materials when doping or aging. Due to its generality, this glass mediated phase transition divergence scheme can be used in other proper material systems to design a desired useful phase transition path for phase transition engineering.

Method

Sample fabrication and processing. The metal alloy samples were cut from $Ti_{49}Ni_{51}$ plates (from Furukawa Electric Co. Ltd.) by spark cutting. The samples were sealed in quartz tubes with a small amount of argon gas before heat treatments. Ti wires were sealed into the tubes to avoid severe oxidation of the samples during heat treatments. The samples were firstly solution treated at 1000 °C for 2 hours and then quenched in water. The samples used in DMA and XRD measurements were aged at 280 °C after sealed in quartz tube for some typical aging times ranging from 10 to 180 min.

Thermal and mechanical characterization. The phase transition was characterized by DSC (Q200 TA Instruments) with cooling/heating rate of 10 °C/min. DMA measurement was carried out in single cantilever mode with frequency range from 0.2 Hz to 20 Hz. To construct the phase diagram of the phase transition, aging process was performed cyclically on the DSC equipment at 280 °C and then the aged sample was characterized by DSC measurement. The longest aging time was 320 min. The size of the samples in DMA measurement is around $0.4 \times 4.0 \times 17.6\,mm^3$. The amplitude was set to $10–15\,\mu m$.

Temperature dependence of X-ray diffraction characterization. The temperature dependence of XRD was performed on Shimadzu XRD7000 equipped with a temperature controller TTK 450 from Anton Paar GmbH to detect the crystalline structure with the temperature.

References

1. Otsuka, K. & Ren, X. Physical metallurgy of Ti-Ni-based shape memory alloys. *Prog. Mater. Sci.* **50,** 511 (2005).
2. Fukuda, T., Saburi, T., Chihara, T. & Tsuzuki, Y. Mechanism of B2-B19-B19' transformation in shape-memory Ti-Ni-Cu alloys. *Mater. Trans. JIM* **36,** 1244 (1995).
3. Fukuda, T., Saburi, T., Doi, K. & Nenno, S. Nucleation and self-accommodation of the R-phase in Ti-Ni alloys. *Mater. Trans. JIM* **33,** 271 (1992).
4. Zhou, Y. M. *et al.* Strain glass in doped $Ti_{50}(Ni_{50-x}D_x)$ (D = Co, Cr, Mn) alloys: Implication for the generality of strain glass in defect-containing ferroelastic systems. *Acta Mater.* **58,** 5433 (2010).
5. Wang, D. *et al.* Strain glass in Fe-doped Ti-Ni. *Acta Mater.* **58,** 6206 (2010).
6. Cui, J. & Ren, X. B. Elinvar effect in Co-doped TiNi strain glass alloys. *Appl. Phys. Lett.* **105,** 061904 (2014).
7. Fan, G. L. *et al.* Origin of abnormal multi-stage martensitic transformation behavior in aged Ni-rich Ti-Ni shape memory alloys. *Acta Mater.* **52,** 4351 (2004).
8. Zhou, Y. M. *et al.* Origin of 2-stage R-phase transformation in low-temperature aged Ni-rich Ti-Ni alloys. *Acta Mater.* **53,** 5365 (2005).
9. Zhang, Z. *et al.* Phase diagram of $Ti_{50-x}Ni_{50+x}$: Crossover from martensite to strain glass. *Phys. Rev. B* **81,** 224102 (2010).
10. Zheng, Y., Jiang, F., Li, L., Yang, H. & Liu, Y. Effect of ageing treatment on the transformation behaviour of Ti-50.9at.%Ni alloy. *Acta Mater.* **56,** 736–745 (2008).
11. Wagner, M.-X. *et al.* Effect of low-temperature precipitation on the transformation characteristics of Ni-rich NiTi shape memory alloys during thermal cycling. *Intermetallics* **18,** 1172–1179 (2010).
12. Kim, J. I. & Miyazaki, S. Effect of nano-scaled precipitates on shape memory behavior of Ti-50.9at.%Ni alloy. *Acta Mater.* **53,** 4545 (2005).
13. Sarkar, S., Ren, X. B. & Otsuka, K. Evidence for strain glass in the ferroelastic-martensitic system $Ti_{50-x}Ni_{50+x}$. *Phys. Rev. Lett.* **95,** 205702 (2005).
14. Zhang, J. *et al.* Spontaneous strain glass to martensite transition in a $Ti_{50}Ni_{44.5}Fe_{5.5}$ strain glass. *Phys. Rev. B* **84,** 214201 (2011).
15. Vogel, H. The temperature dependence law of the viscosity of fluids. *Phys. Z.* **22,** 645 (1921).
16. Fulcher, G. S. Analysis of recent measurements of the viscosity of glasses. *J. Am. Ceram. Soc.* **8,** 339 (1925).
17. Tadaki, T., Nakata, Y., Shimizu, K. & Otsuka, K. Crystal structure, composition and morphology of a precipitate in a aged Ti-51at%Ni Shape memory alloys. *Mater. Trans. JIM* **27,** 731 (1986).
18. Tirry, W. & Schryvers, D. Quantitative determination of strain fields around Ni_4Ti_3 precipitates in NiTi. *Acta Mater.* **53,** 1041–1049 (2005).
19. Tirry, W., Schryvers, D., Jorissen, K. & Lamoen, D. Electron-diffraction structure refinement of Ni_4Ti_3 precipitates in $Ni_{52}Ti_{48}$. *Acta Crystallogr. B* **62,** 966–971 (2006).
20. Khalil-Allafi, J. *et al.* The influence of temperature on lattice parameters of coexisting phases in NiTi shape memory alloys-a neutron diffraction study. *Mater. Sci. Eng. A* **378,** 161–164 (2004).
21. Schryvers, D., Cao, S., Tirry, W., Idrissi, H. & Avert, S. V. Advanced three-dimensional electron microscopy techniques in the quest for better structural and functional materials. *Sci. Technol. Adv. Mater.* **14,** 014206 (2013).

22. Ji, Y., Ding, X., Lookman, T., Otsuka, K. & Ren, X. Heterogeneities and strain glass behavior: Role of nanoscale precipitates in low-temperature-aged $Ti_{48.7}Ni_{51.3}$ alloys. *Phys. Rev. B* **87,** 104110 (2013).
23. Ren, X. B. *et al.* Strain glass in ferroelastic systems: Premartensitic tweed versus strain glass. *Philos. Mag.* **90,** 141 (2010).
24. Tanaka, Y. *et al.* Ferrous polycrystalline shape-memory alloy showing huge superelasticity. *Science* **327,** 1488 (2010).

Acknowledgements

Author Contributions

J.C. designed the experimental scheme and wrote the manuscript. Z.J.Z. and J.C. carried out the experiments. Z.J.Z., J.C. and X.B.R. discussed the results and contributed to writing of the manuscript.

Additional Information

Competing financial interests: The authors declare no competing financial interests.

How to cite this article: Zhou, Z. *et al.* Strain glass state as the boundary of two phase transitions. *Sci. Rep.* **5**, 13377; doi: 10.1038/srep13377 (2015).